ADVANCED MATERIALS
www.advmat.de

Phytochrome-Based Extracellular Matrix with Reversibly Tunable Mechanical Properties

*Maximilian Hörner, Katrin Raute, Barbara Hummel, Josef Madl, Guido Creusen, Oliver S. Thomas, Erik H. Christen, Natascha Hotz, Raphael J. Gübeli, Raphael Engesser, Balder Rebmann, Jasmin Lauer, Bernd Rolauffs, Jens Timmer, Wolfgang W. A. Schamel, Jan Pruszak, Winfried Römer, Matias D. Zurbriggen, Christian Friedrich, Andreas Walther, Susana Minguet, Ritwick Sawarkar, and Wilfried Weber**

Interrogation and control of cellular fate and function using optogenetics is providing revolutionary insights into biology. Optogenetic control of cells is achieved by coupling genetically encoded photoreceptors to cellular effectors and enables unprecedented spatiotemporal control of signaling processes. Here, a fast and reversibly switchable photoreceptor is used to tune the mechanical properties of polymer materials in a fully reversible, wavelength-specific, and dose- and space-controlled manner. By integrating engineered cyanobacterial phytochrome 1 into a poly(ethylene glycol) matrix, hydrogel materials responsive to light in the cell-compatible red/far-red spectrum are synthesized. These materials are applied to study in human mesenchymal stem cells how different mechanosignaling pathways respond to changing mechanical environments and to control the migration of primary immune cells in 3D. This optogenetics-inspired matrix allows fundamental questions of how cells react to dynamic mechanical environments to be addressed. Further, remote control of such matrices can create new opportunities for tissue engineering or provide a basis for optically stimulated drug depots.

The mechanical properties of the extracellular environment govern key cellular decision-making processes such as proliferation, differentiation, or migration.[1] Thus, analyzing how cells gauge and interact with their mechanical environment is critical not only for understanding physiological and pathological processes but also for engineering cell and tissue growth and differentiation in regenerative medicine.[2] Although studies using passive elastic or viscoelastic materials have revealed valuable information about cell–matrix interactions, matrices with adjustable mechanical properties more closely reflect the dynamic environments many cells are exposed to in a living organism.[3] In order to recapitulate these dynamic environments, several materials have been developed, which enable the

Dr. M. Hörner, K. Raute, Dr. J. Madl, O. S. Thomas, Dr. R. Engesser, Prof. J. Timmer, Prof. W. W. A. Schamel, Prof. W. Römer, Dr. S. Minguet, Prof. W. Weber
Signalling Research Centres BIOSS and CIBSS
University of Freiburg
79104 Freiburg, Germany
E-mail: wilfried.weber@biologie.uni-freiburg.de

Dr. M. Hörner, K. Raute, Dr. B. Hummel, Dr. J. Madl, O. S. Thomas, Dr. E. H. Christen, Dr. N. Hotz, Dr. R. J. Gübeli, B. Rebmann, J. Lauer, Prof. W. W. A. Schamel, Prof. W. Römer, Dr. S. Minguet, Prof. W. Weber
Faculty of Biology
University of Freiburg
79104 Freiburg, Germany

Dr. M. Hörner, K. Raute, O. S. Thomas, Dr. N. Hotz, Dr. R. J. Gübeli, Prof. W. W. A. Schamel, Dr. J. Pruszak, Prof. W. Römer, Dr. S. Minguet, Prof. W. Weber
Spemann Graduate School of Biology and Medicine (SGBM)
University of Freiburg
79104 Freiburg, Germany

Dr. B. Hummel, Dr. R. Sawarkar
Max Planck Institute of Immunobiology and Epigenetics
79108 Freiburg, Germany

The ORCID identification number(s) for the author(s) of this article can be found under https://doi.org/10.1002/adma.201806727.

DOI: 10.1002/adma.201806727

G. Creusen, Prof. C. Friedrich, Prof. A. Walther
Institute for Macromolecular Chemistry
FMF Freiburg Materials Research Center
University of Freiburg
79104 Freiburg, Germany

G. Creusen, Prof. W. Römer, Prof. A. Walther
Freiburg Center for Interactive Materials and Bioinspired Technology (FIT)
University of Freiburg
79110 Freiburg, Germany

Dr. R. Engesser, Prof. J. Timmer
Institute of Physics
University of Freiburg
79104 Freiburg, Germany

J. Lauer, Prof. B. Rolauffs
G.E.R.N. Tissue Replacement, Regeneration and Neogenesis
Department of Orthopedics and Trauma Surgery
Medical Center
Faculty of Medicine
University of Freiburg
79085 Freiburg, Germany

Prof. W. W. A. Schamel, Dr. S. Minguet
Centre for Chronic Immunodeficiency (CCI)
Medical Center
University of Freiburg
79104 Freiburg, Germany

 © 2019 WILEY-VCH Verlag GmbH & Co. KGaA, Weinheim

reversible modulation of mechanical properties in response to chemical or optical stimuli.[3a–c,4] Since light as stimulus offers superior spatiotemporal control compared to classical chemical inducers, materials with reversibly adjustable mechanical properties based on sequential photodegradation and photoinitiated crosslinking,[5] *cis–trans* isomerization of azobenzene,[6] guest–host interaction of azobenzene and β-cyclodextrin[7] (all UV and violet light) as well as on the photoreceptors UVR8[8] (UV light), LOV2[9] (blue light), or Dronpa[10] (violet and cyan light) were developed. However, materials that allow fast and fully reversible adjustment of mechanical properties under cell culture conditions with cell-compatible and low energy red light are still lacking. In this study, we have developed such tunable materials by combining design concepts from optogenetics with materials sciences. In optogenetics, phytochrome photoreceptors have evolved as powerful tool as they enable the fast, reversible, dose-dependent, and local control of biological functions.[11] Here, we apply the cyanobacterial photoreceptor Cph1 for the design of biomaterials with mechanical properties that can be reversibly regulated with high spatiotemporal precision by cell-compatible, tissue-penetrating low energy light in the red/far-red spectrum. These dynamic, protein-based biohybrid materials enable interrogation of mechanosignaling processes in mammalian cells.

To develop the optically controlled material, we used the photosensory module of Cph1 (amino acids 1–514) harboring the point mutation Y263F in the chromophore-binding pocket.[12] The Cph1 Y263F mutant is predominantly monomeric in far-red light (≈740 nm) and undergoes a conformational change upon exposure to red light (≈660 nm) that shifts its equilibrium toward the dimeric form.[12] We functionalized the photosensory module with a tandem RGD (Arg-Gly-Asp) motif to allow cell adhesion and with a C-terminal cysteine for coupling to vinylsulfone (VS)-functionalized 8-arm poly(ethylene glycol) (PEG) via Michael-type addition (**Figure 1**a). In this configuration, illumination with 660 nm light is expected to increase the crosslink density in the PEG network and therefore the stiffness of the material. In contrast, illumination with 740 nm light should reduce the number of crosslinks and soften the material.

We produced this Cph1 variant (designated Cph1*) in an *E. coli* strain harboring genes for the biosynthesis of the Cph1* chromophore phycocyanobilin (PCB).[12] We purified the protein by immobilized metal affinity chromatography and confirmed its identity by Western blotting and by Zn^{2+}-staining of the Cph1*-ligated PCB (Figure S1a, Supporting Information). Photoconversion of Cph1* was confirmed by measuring the absorbance spectra upon illumination with 660 or 740 nm light (Figure S1b, Supporting Information). We used size exclusion chromatography to characterize the light-responsive dimerization of Cph1* and revealed that the dimer-to-monomer ratio gradually decreased with increasing illumination wavelength (Figure S1c,d, Supporting Information). The dissociation constant under 660 or 740 nm light was $K_D = 5.6 \times 10^{-6}$ M (95% confidence interval (CI): [3.4×10^{-6} M, 9.0×10^{-6} M]) or $K_D = 1.7 \times 10^{-3}$ M (95% CI: [0.74×10^{-3} M, 5.5×10^{-3} M]), respectively (Figure S1e, Supporting Information).

We next synthesized hydrogels by reacting increasing concentrations of Cph1* (50–140 mg mL^{-1}, final Cph1* concentration) with VS-functionalized 8-arm PEG (PEG-VS, 40 kDa) at a molar VS:Cph1* ratio of 2:1. After gelation at 23 °C under nitrogen for 20 h, the elasticity of the hydrogels was evaluated by determining the storage modulus G'. G' of the resulting hydrogels increased with increasing Cph1* concentrations and G' was always higher at 660 nm light compared to 740 nm light (Figure 1b and Figure S2, Supporting Information). Hydrogels synthesized from 70 mg mL^{-1} Cph1* were chosen for further characterization since they showed the highest reversible, light-responsive dynamic change in G' (Figure S2, Supporting Information) within the range where cells gauge their environment.[3f]

To further characterize the bonds that formed the hydrogel, we incubated the gels for 96 h in either sodium dodecyl sulfate (SDS, to denature Cph1* and to disrupt Cph1* dimers) or in trypsin (to digest Cph1*). Incubation in SDS resulted in the swelling of the gels whereas trypsin triggered gel dissolution (Figure S3a, Supporting Information). These observations indicate the presence of additional covalent polymer–protein bonds beyond the terminal cysteine. Analysis of the crystal structure of Cph1 revealed one additional free cysteine (Cys371), 14 lysines, and the Cph1* N-terminus on the surface as potential coupling sites for VS (see Note S1, Supporting Information).[12] NMR analysis of PEG-VS incubated with cysteine and lysine at a molar ratio similar as the one on the protein surface revealed that PEG-VS reacted highly specific with cysteines and had only minor reactivity toward lysines under the coupling conditions used in this study (see Note S1, Supporting Information). This suggests that additional crosslinks between PEG-VS and the Cph1-internal surface-exposed Cys371 might further stabilize the hydrogel and prevent its dissolution under 740 nm light.

Cph1* retained its photoswitchable properties after gel synthesis, as observed by measuring the absorbance of the hydrogels following illumination at 660 or 740 nm (Figure S3b, Supporting Information). The light-induced change in Cph1* correlated with changes in storage and loss moduli, as characterized by amplitude and frequency sweep experiments (Figure S3c, Supporting Information). For both illumination conditions, gel properties ($G' > G''$) prevailed over the measured frequency range (0.01–1 Hz). Further, the stress relaxation properties of the hydrogel were shown to be photoresponsive. The relaxation time $t_{1/2}$ was determined as the time at which

Dr. J. Pruszak
Institute of Anatomy and Cell Biology
Department of Molecular Embryology
Faculty of Medicine
University of Freiburg
79104 Freiburg, Germany

Prof. M. D. Zurbriggen
Institute of Synthetic Biology and CEPLAS
Heinrich Heine University Düsseldorf
40204 Düsseldorf, Germany

Prof. A. Walther
Cluster of Excellence Living, Adaptive and Energy-Autonomous Materials Systems (livMatS)
University of Freiburg
79110 Freiburg, Germany

Dr. R. Sawarkar
CIBSS - Centre for Integrative Biological Signalling Studies
University of Freiburg
79104 Freiburg, Germany

 © 2019 WILEY-VCH Verlag GmbH & Co. KGaA, Weinheim

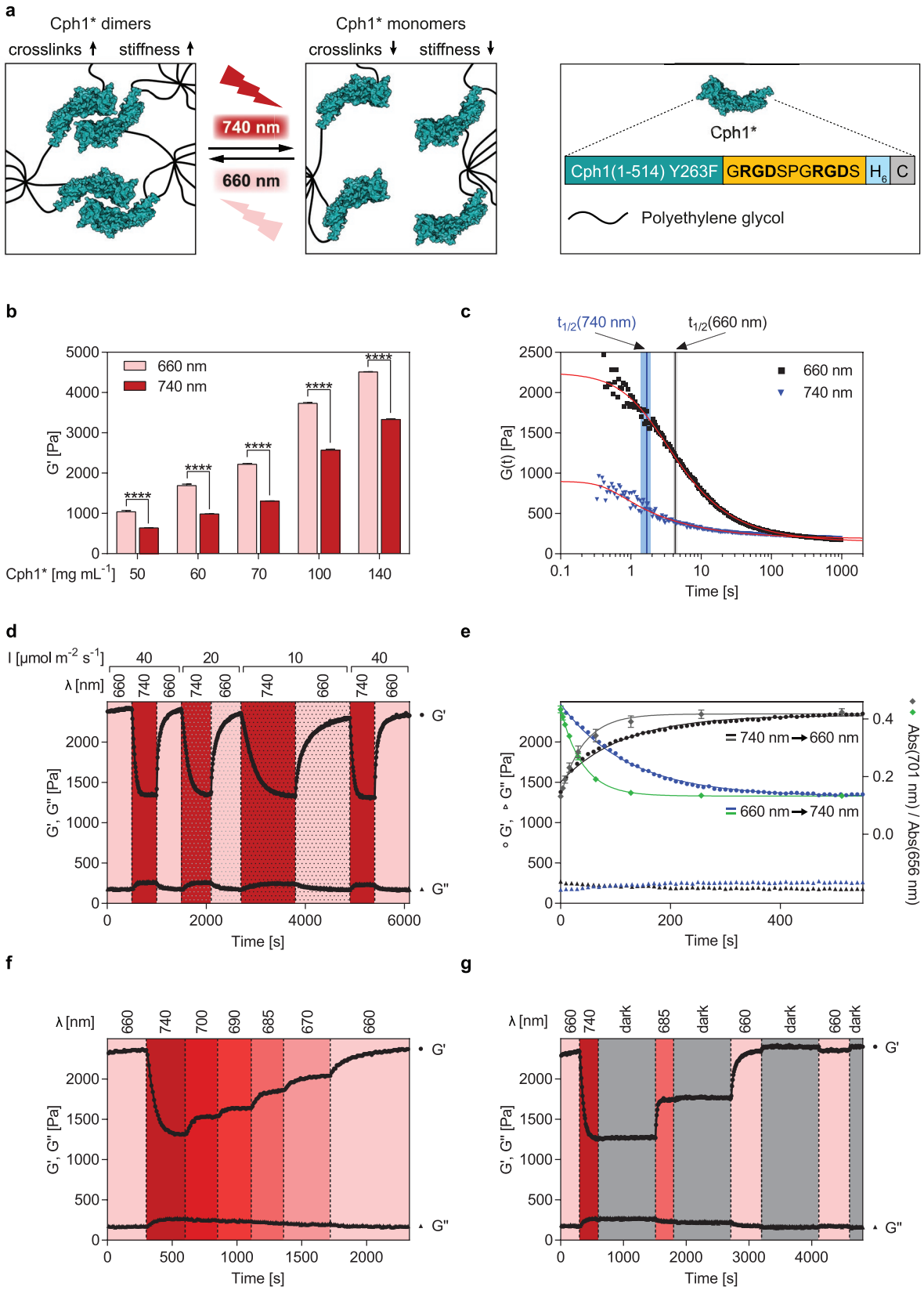

Figure 1. Design and characterization of the phytochrome-based hydrogel. a) Cph1* is covalently coupled to branched 8-arm poly(ethylene glycol) (PEG). Illumination at 660 nm triggers formation of Cph1*-dimer-based polymer crosslinks, whereas 740 nm light shifts the Cph1* equilibrium to the monomeric state, resulting in reduced polymer crosslink density. Cph1* comprises amino acids 1–514 of wild type Cph1, and contains the point

© 2019 WILEY-VCH Verlag GmbH & Co. KGaA, Weinheim

the relaxation modulus $G(t)$ relaxed to half of its dynamic range: $G(t_{1/2}) = G_{inf} + (\Delta G/2)$. Under 660 nm illumination we obtained $t_{1/2}$ = 4.3 s (95% CI: [4.0 s, 4.5 s]), whereas 740 nm light yielded in a significantly faster relaxation with $t_{1/2}$ = 1.7 s (95% CI: [1.4 s, 1.9 s]) (Figure 1c and Figure S3d, Supporting Information).

To comprehensively characterize the photoreceptor-based hydrogels, we evaluated whether they shared the hallmarks of biological optogenetic systems, in which the output signal is i) fully reversible by alternating the illumination input, ii) dose-dependent by adjusting the light flux, iii) adjustable by different illumination wavelengths, and iv) subject to precise spatial control.[11a] Reversibility and dose dependency were evaluated by tracing the storage (G') and loss (G'') moduli under alternating illumination with 660 or 740 nm light at a photon flux intensity of 40, 20, and 10 µmol m^{-2} s^{-1} (Figure 1d). A shift to 740 nm light induced a decrease of G' by 44%, which was fully reversible by subsequent illumination with 660 nm light. Decreasing light intensities resulted in slower switching kinetics (Figure 1d). Tracing photoconversion of Cph1* in the hydrogel revealed that 50% of Cph1* was converted within $t_{1/2}$ = 31 s (95% CI: [22 s, 39 s]) or $t_{1/2}$ = 28 s (95% CI: [24 s, 32 s]) when switching from 740 to 660 nm light or vice versa, respectively (20 µmol m^{-2} s^{-1} for either wavelength, Figure 1e). Changes in G' slightly lagged behind photoconversion with $t_{1/2}$ = 78 s (95% CI: [72 s, 85 s]) or $t_{1/2}$ = 86 s (95% CI: [82 s, 89 s]) for the respective switching in illumination wavelength (Figure 1e). We next characterized the reproducibility of the switching process. To this aim, hydrogels were subjected to 144 illumination cycles, each cycle consisting of 10 min 660 nm light and 10 min 740 nm light (20 µmol m^{-2} s^{-1}) prior to measuring G' for one additional cycle (Figure S4a, Supporting Information). The switching behavior of those gels was not different to gels that were continuously illuminated for 48 h at 660 or 740 nm, indicating that the functionality of the hydrogels was highly robust over time and was not influenced by repeated switching. The reversible switching behavior was compatible with different commonly used cell culture media and highly reproducible from one hydrogel synthesis batch to the other (Figure S4b,c, Supporting Information).

To characterize the influence of light color on G', we gradually changed the illumination wavelength from 740 to 660 nm. The concomitant gradual increase in G' suggests that any intermediate stiffness can be set by choosing the appropriate illumination color (Figure 1f). A similar gradual adjustment of G' was achieved by mixing 660 and 740 nm light at different intensities, obviating the need for wavelength-specific illumination devices when aiming for intermediate G' (Figure S4d, Supporting Information). The hydrogels maintained the preset G' in the dark (Figure 1g). No change in the Cph1* photostate was observed in the dark during 24 h (Figure S4e, Supporting Information) which is in agreement with a reported half-life time for Cph1 dark reversion of $t_{1/2}$ > 264 h.[12] All rheological characterization experiments shown in Figure 1c–g were performed with hydrogels of a thickness of 300 µm and low light intensities (≤40 µmol m^{-2} s^{-1}). To control thicker gels with the same kinetics, higher light intensities could be used. For example, during live cell imaging in another study, light intensities up to 3650 and 1850 µmol m^{-2} s^{-1} for 625 and 740 nm illumination were used, respectively.[13]

We next explored the possibility of changing the local mechanical properties of the material. To this end, we first mapped the hydrogel surface by indentation-type atomic force microscopy (AFM), which revealed a significant decrease in the mean Young's modulus upon switching from 660 to 740 nm light (**Figure 2**a and Figure S5a, Supporting Information). The heterogeneity of the hydrogel surface was shown to be comparable to the one of fibrin gels (Figure S5b, Supporting Information) and natural tissues.[14] We next illuminated a hydrogel in the AFM using the attached white light source (2 µmol m^{-2} s^{-1}), which was shown to have the same influence on Cph1* as illumination with 660 nm light (Figure S5c, Supporting Information). Additional projection of a circular pattern of 740 nm light (400 µmol m^{-2} s^{-1}, 0.6 mm diameter) resulted in a local decrease in the Young's modulus, indicating that mechanical gradients can be established (Figure 2b and Figure S5d,e, Supporting Information). Subsequently switching off the 740 nm light source resulted in the homogenous restiffening of the gel surface. Based on our previous work with the related Arabidopsis phytochrome B, we suggest that the spatial resolution of stiffness modulations could be increased to the µm range using a confocal microscope equipped with a red (e.g., 633 or 660 nm) and/or far-red (e.g., 740 nm) laser.[15]

mutation Y263F for light-inducible dimerization, a tandem RGD-based integrin attachment signal, a hexahistidine tag (H_6) for purification, and a C-terminal cysteine for coupling to vinylsulfone-functionalized 8-arm PEG. Structure of Cph1, PDB ID: 3ZQ5. b–g) Unless stated otherwise, hydrogels were synthesized from 70 mg mL^{-1} Cph1* and illumination intensity was 40 µmol m^{-2} s^{-1}. Gels were equilibrated for 24 h and analyzed in cell culture medium containing 10% fetal calf serum (FCS) at 37 °C. Storage (G') and loss (G'') moduli were determined by small amplitude oscillatory shear rheology with a frequency of 1 Hz and a deformation of 0.5%. b) Influence of Cph1* concentration on G' after 10 min illumination with 660 or 740 nm light. Mean ± s.d. of n = 10–18 technical replicates, ****$P < 0.0001$. c) Light-dependent stress relaxation. The relaxation modulus $G(t)$ of gels previously illuminated for 10 min with 660 or 740 nm light was traced upon an initial deformation of 10%. The relaxation time $t_{1/2}$ at which $G(t)$ relaxed to half of its dynamic range (vertical lines with 95% confidence intervals) was determined by fitting $G(t)$ of n = 4 replicates to a stress-relaxation model (red lines, Figure S3d, Supporting Information). Data points of one representative experiment are shown. d) Reversible and dose-dependent switching of G' and G'' by illumination with the indicated intensities (I) and wavelengths. e) Kinetics of Cph1* photoconversion and G' following optical switching. Hydrogels were illuminated with 660 or 740 nm light for 10 min (20 µmol m^{-2} s^{-1}) prior to swapping the illumination wavelength. Photoconversion of Cph1* was analyzed by tracing the ratio of hydrogel absorbance at 701 and 656 nm. Solid curves are derived from a model assuming linear transition rates between the different states, which were used to determine the conversion times described in the main text. Absorbance ratios represent the mean ± s.d. of n = 6 hydrogels. The corresponding time course of G' and G'' is indicated. f) Adjustment of G' and G'' by wavelength-specific illumination. The hydrogel was successively illuminated at the indicated wavelengths (15 µmol m^{-2} s^{-1} except for the initial 660/740 nm cycle) while recording G' and G''. g) Persistence of light-adjusted G' and G'' in the dark. The hydrogel was illuminated at the indicated wavelengths or kept in the dark while tracing G' and G''. The thickness of the hydrogels in (c)–(g) was 300 µm. Rheological data in (d)–(g) are representative data from at least n = 3 replicates.

© 2019 WILEY-VCH Verlag GmbH & Co. KGaA, Weinheim

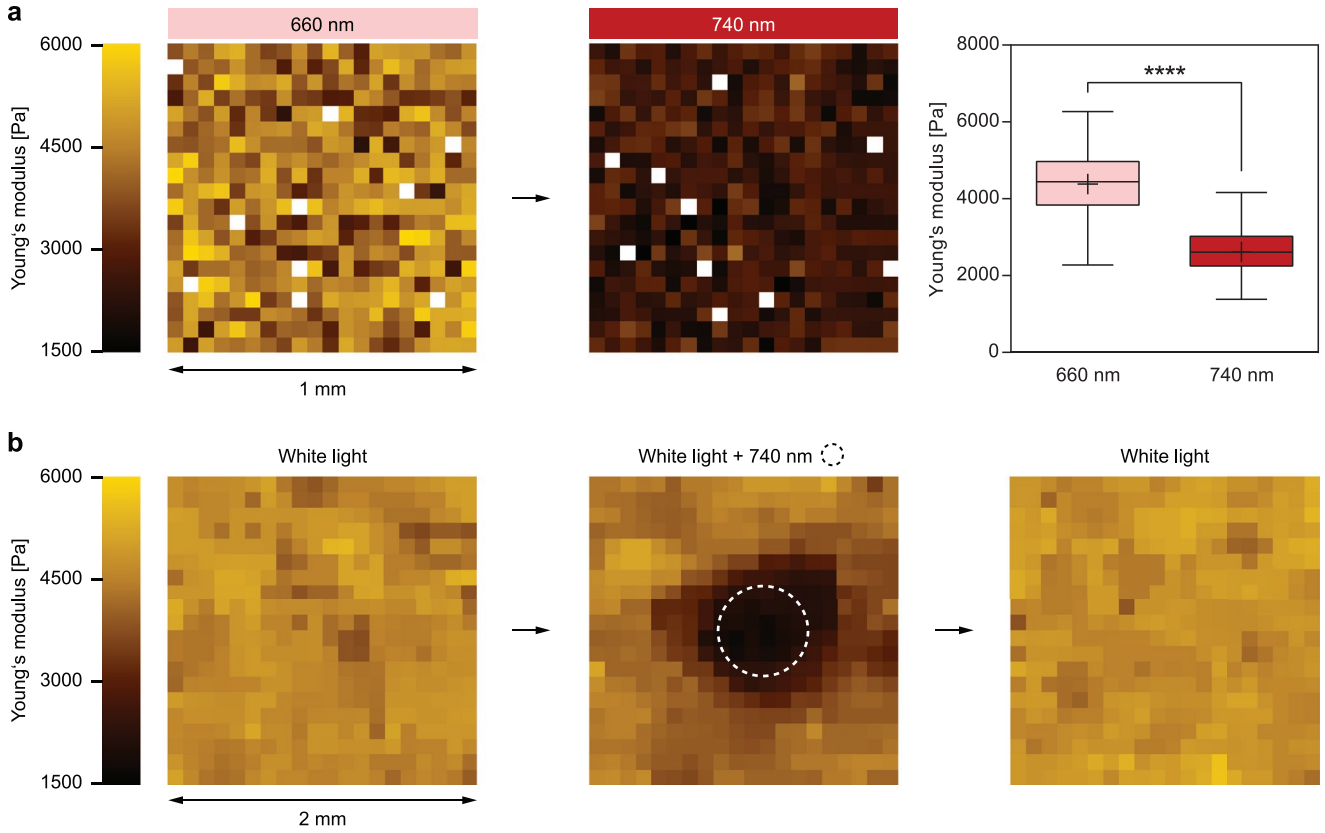

Figure 2. Precise spatiotemporal control of mechanical properties of the phytochrome-based hydrogels. a) Spatial distribution of the Young's modulus of the surface of hydrogels synthesized from 70 mg mL^{-1} Cph1* after illumination with 660 nm (5 min, 80 µmol m^{-2} s^{-1}) or 740 nm (5 min, 400 µmol m^{-2} s^{-1}) light. Stiffness maps were recorded by atomic force microscopy (AFM) by 20 × 20 force–distance curves measured on a regular grid pattern with 50 µm spacing. Positions where the approach curve could not be fitted via a simple Hertz indentation model are shown as white points. Right panel: Distribution of the Young's modulus. For 660 and 740 nm illumination, the mean ± s.d. is 4.4 ± 0.8 kPa (relative s.d.: 18%) and 2.6 ± 0.5 kPa (relative s.d.: 19%), respectively. ****$P < 0.0001$. Representative data of $n = 3$ replicates are shown. b) Local softening of the hydrogel by patterned illumination. The hydrogel (as above) was illuminated for 5 min with white light (20 µmol m^{-2} s^{-1}, white light has the same effect as 660 nm light, Figure S5c, Supporting Information) and the Young's modulus was mapped on a regular 20 × 20 grid pattern with 100 µm spacing (left panel). Subsequently, the hydrogel was additionally locally illuminated with 740 nm light through a circular photomask (diameter: 0.6 mm, 400 µmol m^{-2} s^{-1}, dashed white circle) for 5 min prior to rescanning the hydrogel (middle panel). Finally, the hydrogel was illuminated exclusively with white light for 5 min and another scan was performed (right panel). The stiffness maps were median filtered to substitute for curves that had to be rejected due to a deviation from the Hertz model. Unfiltered data and statistical analysis are shown in Figure S5d,e in the Supporting Information.

We then characterized the illumination-dependent pore sizes of the gels by three complementary methods. First, we incubated gels with fluorescently labeled probes and analyzed their penetration into the gel (Figure S6, Supporting Information). While large particles ($r \geq 0.5$ µm) were unable to enter the gels, pure dye molecules and polymer-tethered dye molecules (fluorescein isothiocyanate (FITC)-dextrans) showed a size-dependent uptake. Second, we calculated the pore sizes based on hydrogel swelling (see Note S2, Supporting Information). These analyses revealed a range for the pore sizes under 660 nm illumination of 28–94 nm or 26–89 nm for the hydrogels synthesized from 50 or 70 mg mL^{-1} Cph1*, respectively. Upon 740 nm illumination, the pore size increased by less than 10%. Third, we calculated the pore sizes of the hydrogel synthesized from 50 mg mL^{-1} Cph1* (as later used for migration experiments) from the diffusion of 2 MDa FITC-dextran as determined by fluorescence recovery after photobleaching (FRAP) experiments (see Note S2, Supporting Information). In accordance with the previous analyses, we determined a pore size of ≈59 or ≈70 nm under 660 or 740 nm illumination, respectively (increase of ≈19% upon 740 nm illumination). In summary, these pore sizes are substantially smaller than required to be exploitable for migration of mammalian T cells[16] as discussed below.

Next, we evaluated the suitability of the phytochrome-based hydrogels as cell growth matrix. Primary human mesenchymal stem cells (hMSCs) cultivated on the gels adhered and spread (**Figure 3**a and Figure S7a, Supporting Information). This spreading can be attributed to the RGD motif in Cph1* as poor spreading was observed on gels synthesized from Cph1* in which the RGD motif had been deleted or replaced by a scrambled RGD sequence (RDG, Figure S7a, Supporting Information).[17] Cultivating hMSCs on phytochrome-based hydrogels illuminated for 2 h with 660 or 740 nm light followed by 46 h cultivation in the dark revealed that cells on gels illuminated with 660 nm light showed a larger cell area compared to cells on gels exposed to 740 nm light (Figure 3b). Cell spreading is known to depend on the mechanical properties of the matrix

© 2019 WILEY-VCH Verlag GmbH & Co. KGaA, Weinheim

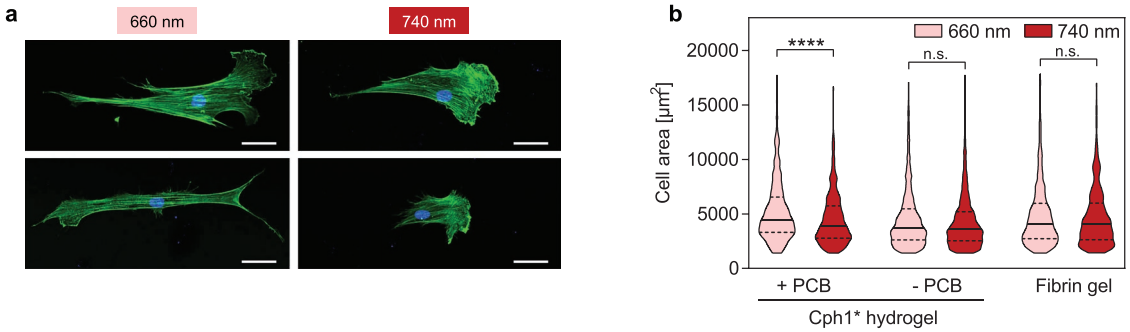

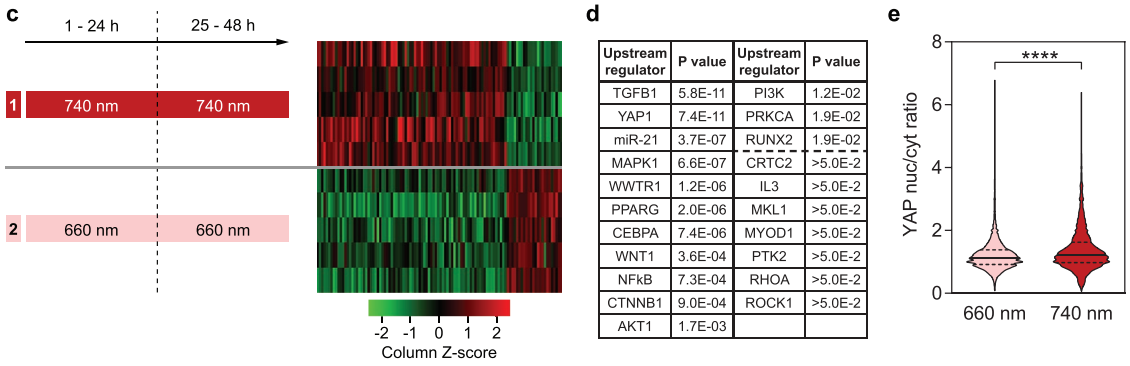

Upstream regulator	P value	Upstream regulator	P value
TGFB1	5.8E-11	PI3K	1.2E-02
YAP1	7.4E-11	PRKCA	1.9E-02
miR-21	3.7E-07	RUNX2	1.9E-02
MAPK1	6.6E-07	CRTC2	>5.0E-2
WWTR1	1.2E-06	IL3	>5.0E-2
PPARG	2.0E-06	MKL1	>5.0E-2
CEBPA	7.4E-06	MYOD1	>5.0E-2
WNT1	3.6E-04	PTK2	>5.0E-2
NFkB	7.3E-04	RHOA	>5.0E-2
CTNNB1	9.0E-04	ROCK1	>5.0E-2
AKT1	1.7E-03		

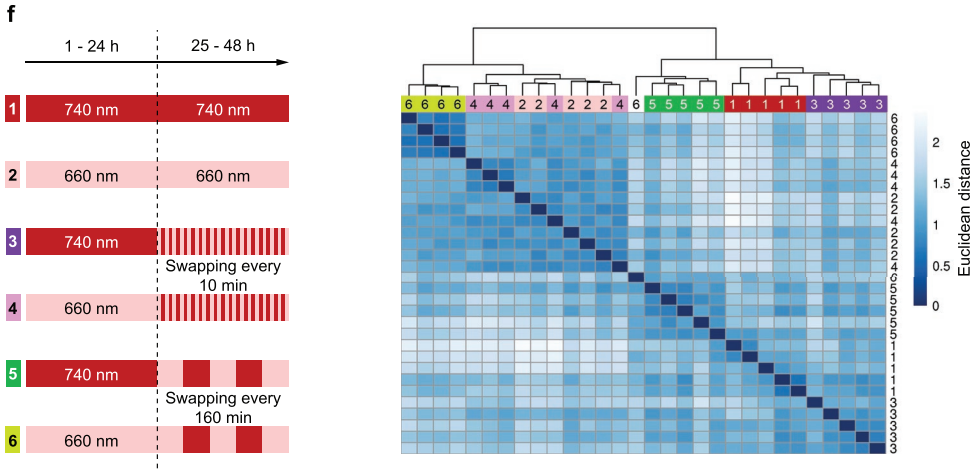

g

Clustering pattern	(i)	(ii)	(iii)	(iv)
Clustering scheme	1 3 5 2 4 6	1 3 2 4 5 6	3 4 5 6	1 3 5 2 4 6
Pathways	all 106 differentially expressed genes	PPARG WWTR1 PRKCA AKT1 CTNNB1 NFkB PI3K	CEBPA MAPK1	TGFB1 YAP1 miR-21 RUNX2 WNT1

Figure 3. Mechanosignaling-induced transcriptional reprogramming triggered by dynamic mechanical environments. For all experiments hydrogels synthesized from 70 mg mL^{-1} Cph1* were used. Illumination intensity was 20 µmol m^{-2} s^{-1}. a) Phytochrome-based hydrogels as cell culture matrix. hMSCs were cultivated at low density (2000 cells cm^{-2}) on phytochrome-based hydrogels. Samples were illuminated at 660 or 740 nm for 2 h and subsequently kept in the dark for 46 h prior to 4′,6-diamidino-2-phenylindole (DAPI) (blue, nuclei)/Phalloidin (green, actin) staining and visualization by confocal microscopy. Scale bars: 50 µm. b) Area of cells cultivated under the conditions described in (a). As controls, fibrin gels or non-photoresponsive

© 2019 WILEY-VCH Verlag GmbH & Co. KGaA, Weinheim

such as stiffness or stress relaxation but also on parameters like ligand or cell density.[18] For example, it was reported using elastic materials that cell spreading was increased with a higher stiffness of the matrix, whereas on stress relaxing materials this effect was less pronounced.[18c] Interestingly, on soft gels with stress relaxing properties higher cell areas were observed compared to purely elastic gels whereas an inverse effect was described at higher stiffnesses.[18c] Further, higher cell densities were suggested to override the effect of matrix stiffness on cell spreading.[18e] We hypothesize that under our experimental conditions the increased spreading area might be induced by the higher stiffness under 660 nm light. To exclude that illumination directly influenced cell area, we performed parallel experiments on fibrin gels or on gels synthesized from Cph1* produced in the absence of PCB chromophore biosynthesis genes. The storage modulus of the chromophore-devoid Cph1* gels did not change in response to illumination (Figure S7b, Supporting Information). Cells cultivated on the control gels under the aforementioned illumination conditions did not show a wavelength-dependent difference in cell area (Figure 3b). Similarly, potential illumination-associated temperature effects on cells can likely be excluded, given that the maximum temperature difference between illumination at 660 and 740 nm was less than 0.15 K (Figure S7c, Supporting Information).

In order to determine whether the differences in the hydrogel mechanical properties were accompanied by changes in global gene expression, we performed RNA sequencing (RNA-seq) analysis of hMSCs cultivated under different static and dynamic mechanical conditions. First, we cultivated hMSCs on phytochrome-based hydrogels for 48 h under constant 660 or 740 nm light. As a control, we cultivated hMSCs under the same illumination conditions on non-photoresponsive gels synthesized from Cph1* devoid of the chromophore PCB. Subsequently, cells were harvested and genome-wide RNA-seq revealed 106 genes to be differentially expressed on the phytochrome-based hydrogels (Figure 3c, and Figure S7d and Table S1, Supporting Information). These genes showed a significant overlap ($P < 0.05$) with target genes of 14 signaling pathways and upstream regulators previously associated with mechanosignaling in hMSCs (Figure 3d).[19] Seven signaling pathways that have further been associated with mechanosignaling, such as IL3 or MyoD1 showed a nonsignificant overlap of target genes.[19] For example, illumination at 740 nm resulted in the upregulation of target genes of yes-associated protein (YAP), a key transcriptional coactivator involved in mechanotransduction (Table S1, Supporting Information). In agreement with these RNA-seq findings, the YAP nuclear-to-cytoplasmic distribution was higher in cells cultivated on gels illuminated with 740 nm compared to gels under 660 nm light (Figure 3e). The nuclear localization of YAP was reported to depend on matrix stiffness, stress relaxation, and on cell density.[18c,d,20] For example, it was described that a higher stiffness correlated with an increase in the nuclear fraction of YAP.[20] Similarly, when using matrices of the same stiffness but with different stress relaxation, a faster stress relaxation correlated with increased nuclear YAP.[18c,d] In addition, higher cell densities were observed to correlate with a lower fraction of nuclear YAP.[20a] The increased nuclear localization of YAP under 740 nm illumination could indicate that in our experimental configuration the faster stress relaxation under 740 nm light may have outweighed the YAP deactivating effect of concomitantly decreased G' (Figure 1c,d).

To determine whether altering the mechanical environment resulted in changes in cellular gene expression, we first incubated hMSCs on hydrogels under 660 nm illumination for 24 h, followed by another 24 h under 740 nm light. Subsequently, we switched to 660 nm light for 0, 10, 40, or 160 min prior to analyzing the transcriptome (Figure S7e, Supporting Information). Cells cultivated for 0, 10, or 40 min under 660 nm light did not show differentially expressed genes. However, after 160 min cultivation at 660 nm, the gene expression profile resembled the one of cells continuously cultivated under 660 nm light. To rule out that the observed changes in gene expression were caused by differential display of the RGD motif on the Cph1* monomer or dimer under either illumination wavelength, we performed the following control experiment: hMSCs cultivated on a glass surface functionalized with Cph1* via a PEG linker (5 kDa) displayed no changes in gene expression in response to the illumination conditions used as controls in Figure S7e (Figure S7f,g, Supporting Information).

A key process in mechanosignaling-induced cell fate decisions is the ability of cells to memorize a previous mechanical environment.[3f,19c] While pioneering studies investigated the mechanical memory upon transferring cells from a stiff to a soft substrate or vice versa,[3f,19c,21] it remains elusive how cells differentiate between fluctuating mechanical cues as sporadically occurring during normal physiological processes (e.g., muscle contraction, sporadic external forces) and long-lasting cues (such as present within a given tissue) that might determine cell fate decisions.

gels synthesized from Cph1* devoid of the chromophore PCB were used. Median, solid lines. Upper and lower quartiles, dashed lines. ****$P < 0.0001$. n.s., not significant: $P > 0.05$. $n > 700$ cells per condition. c) Transcriptional profile of hMSCs (26 000 cells cm^{-2}) cultivated for 48 h under constant 740 or 660 nm light. Genome-wide RNA-seq revealed 106 differentially expressed genes ($P < 0.05$, Table S1 and Figure S7d, Supporting Information). Normalized expression values of these 106 genes are depicted in the heat map ($n = 5$ biological replicates are shown). d) List of selected pathways previously associated with mechanosignaling in hMSCs. The overlap of target genes of those pathways with the differentially expressed genes (c) is indicated by the corresponding *P*-value. The dashed line indicates the $P < 0.05$ threshold. e) Nuclear/cytoplasmic distribution of YAP in hMSC cultivated as in (c). Median, solid lines. Upper and lower quartiles, dashed lines. ****$P < 0.0001$. $n > 5600$ cells per condition. f) Characterization of the mechanical memory under fluctuating mechanical stimuli. hMSCs (26 000 cells cm^{-2}) were incubated under the indicated illumination schemes and the corresponding transcriptional profiles were analyzed by unsupervised hierarchical clustering (based on the 106 genes in Table S1, Supporting Information). The Euclidean distance across $n = 5$ biological replicates of each condition is indicated by blue color code. Clustering of replicates from the same condition is highlighted by colored condition numbers. g) Mechanical memory behavior of selected mechanosignaling pathways ((d) with $P < 0.05$). The expression of target genes related to the indicated signaling pathways was analyzed by unsupervised hierarchical clustering (Figure S8, Supporting Information). The signaling pathways were grouped according to their different mechanical memory behavior, as represented by the different clustering schemes.

© 2019 WILEY-VCH Verlag GmbH & Co. KGaA, Weinheim

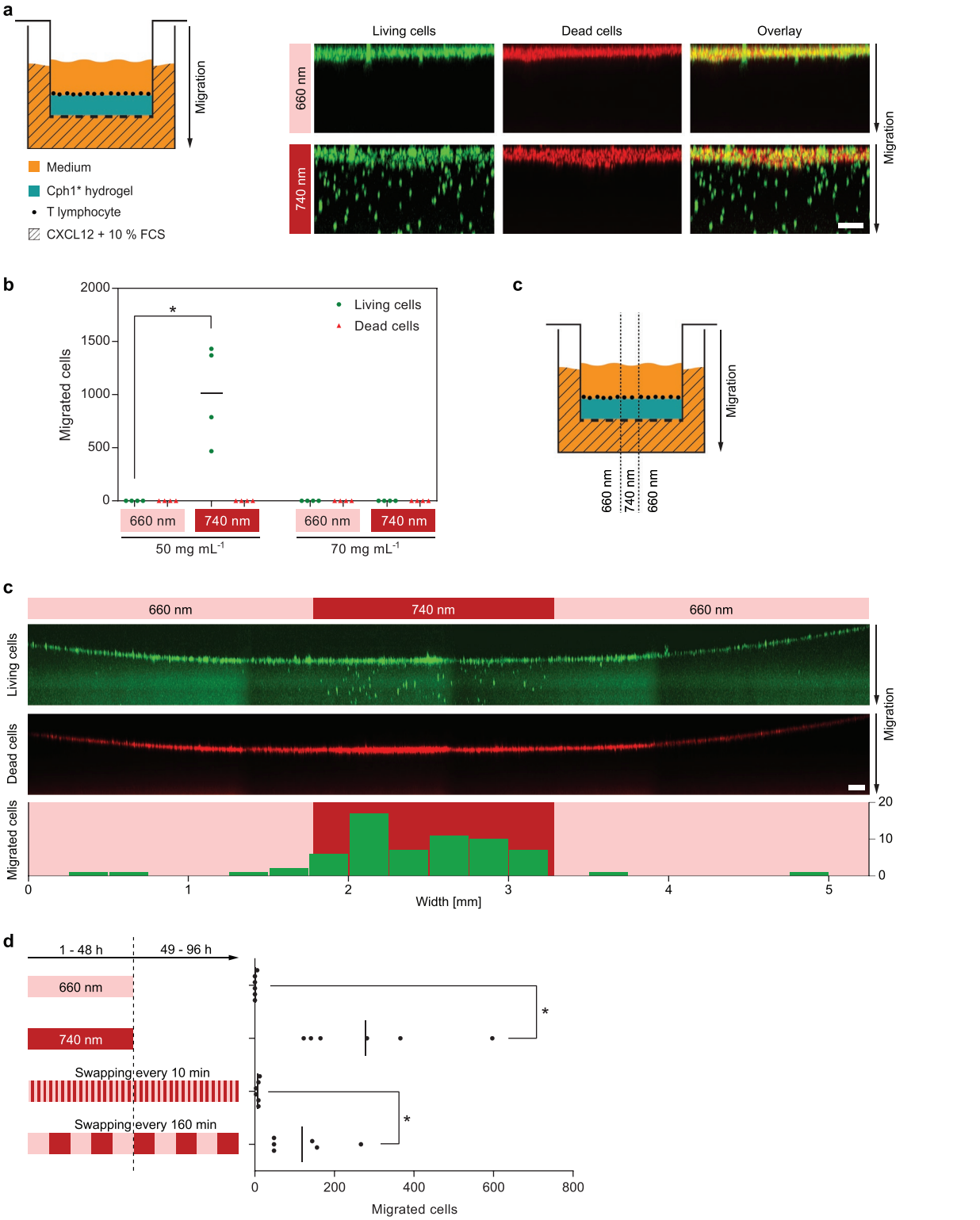

Figure 4. Optical control of T lymphocyte migration. If not stated otherwise, hydrogels synthesized from 50 mg mL^{-1} Cph1* were used. One representative experiment of three independent experiments is shown. a) Light-controlled cell migration. Phytochrome-based hydrogels were cast in a transwell insert, overlaid with cell culture medium containing 2% FCS and placed in a well containing medium supplemented with 10% FCS and the chemoattractant CXCL12. Living (carboxyfluorescein succinimidyl ester (CFSE)-stained, green) and dead (formaldehyde-fixed, CellTrace Yellow-stained, red) primary activated murine T lymphocytes were placed on top of the gels. Cells were cultivated for 8 h under 660 or 740 nm light (40 µmol m^{-2} s^{-1}) prior to confocal imaging of the hydrogels. Scale bar: 100 µm. b) Flow cytometry-based analysis of cell migration after 24 h as described in (a). Number and fluorescence of cells migrated into the lower wells were analyzed by flow cytometry. $n = 4$ biological replicates. Mean is indicated. *$P < 0.05$.

© 2019 WILEY-VCH Verlag GmbH & Co. KGaA, Weinheim

To address this question, we cultivated hMSCs on the phytochrome-based hydrogels under oscillating light conditions (Figure 3f). First, we primed hMSCs for 24 h by cultivation under either 740 nm light (conditions 1, 3, and 5) or 660 nm light (conditions 2, 4, and 6) before we switched illumination (between 660 and 740 nm, with all experiments finished at 660 nm) either every 10 min (conditions 3 and 4) or every 160 min (conditions 5 and 6) for another 24 h. Samples illuminated for another 24 h at constant 740 nm (condition 1) or 660 nm (condition 2) light served as controls. The samples were analyzed by RNA-seq and clustered based on the Euclidian distance between the expression levels of the 106 genes differentially expressed under constant 740 nm (condition 1) and 660 nm (condition 2) light (Figure 3c,f). We found that samples illuminated at the same wavelength for the first 24 h clustered together (conditions 1, 3, and 5 vs conditions 2, 4, and 6). Within either cluster, the samples under continuous and fast changing (every 10 min) illumination clustered together (defined as clustering pattern (i) in Figure 3g), suggesting that fast fluctuations have a lower influence on mechanoresponsive transcriptional changes than more persistent changes (160 min) in matrix stiffness.

To analyze by which signaling pathways hMSCs could discriminate transient fluctuations in mechanical cues from persistent mechanical conditions, we restricted the clustering analysis of Figure 3f to signaling pathway-specific target genes showing differential expression at constant 660 or 740 nm illumination (Figure 3d, $P < 0.05$). This clustering analysis revealed three additional categories of how hMSCs interpreted changing mechanical environments in our setup (Figure 3g and Figure S8, Supporting Information): ii) Observation of two clusters, the first one comprising conditions 1 and 3 and the second one comprising conditions 2, 4, 5 and 6 indicates that the corresponding signaling pathways were robust to transient fluctuations at the minutes scale (10 min) whereas they responded to mechanical cues in the hours range (160 min). iii) Clustering of condition 3 with 4 in one subcluster and of condition 5 with 6 in a second subcluster indicates that pathway-responsive gene expression was mainly influenced by mechanical conditions of the recent 24 h (time period 25–48 h) and that the underlying pathways did not exhibit memory across this time span. Such a configuration was observed, for example, for the mitogen-activated protein (MAP) kinase pathway (MAPK1). iv) Contrarily, clustering of conditions 1, 3, and 5 in one subcluster and of conditions 2, 4, and 6 in a second subcluster suggests that the signaling events were largely influenced by the first 24 h priming period and not by the more recent mechanical cues in the second 24 h. Such mechanical memory is important for maintaining persistent mechanoresponsive signaling that is resistant to transient mechanical fluctuations at the minutes to hours scale. This was the case for YAP and microRNA-21 (miR-21, a central regulator of fibrotic cell program), both of which were shown to be involved in long-term mechanical memory (days to weeks).[3f,19c] These analyses provide the basis to mechanistically elucidate how transient and persistent cues are differentially interpreted by the cell in order to control mechanoresponsive cellular programs.

The mechanical environment of a cell does not only determine signaling processes that control cell fate decisions, it also represents a key parameter controlling cell migration.[1b] Highly mobile lymphocytes of the immune system encounter dramatically different microenvironments within short time frames: from relatively soft healthy lymphoid tissues with an elastic modulus of ≈120 Pa, to healthy or diseased microenvironments, in which the elastic modulus increases up to ≈1000 kPa.[22] Activated T cells migrate from the lymph node to the circulation, and then across the vascular endothelium and basement membrane into peripheral tissues, wherein they follow chemokine gradients. The impact of matrix stiffness on T cell migration has recently been analyzed in 2D on substrates of different stiffness. For example, it was shown on polyacrylamide matrices that T cell migration is faster on stiffer (100 kPa) surfaces compared to softer (0.5–6.4 kPa) ones.[23] Further, T cells migrating on cell monolayers of different stiffness were seeking for softer regions for leukodiapedesis, a process termed tenertaxis.[24] However, despite the importance of T cell migration through tissues with diverse mechanical environments,[22b] it remains poorly understood how the mechanical properties of a 3D environment impact on T cell migration. To address this question, we first evaluated the suitability of the phytochrome-based hydrogels as an optically controlled matrix for T cell migration. Primary activated murine T cells were allowed to migrate toward CXCL12/FCS across hydrogels (50 mg mL^{-1} Cph1*) in a transwell configuration (**Figure 4**a). After 48 h we performed microscopical analysis and counted the cells migrated into the lower reservoir by flow cytometry (Figure 4a,b). This analysis revealed that T cells were able to migrate through gels illuminated with 740 nm light whereas illumination with 660 nm light restricted T cell migration. In order to confirm that the observed migration was an active process, we performed control experiments with formaldehyde-fixed cells (termed "dead cells"). Fixed cells were not able to enter into the gels under any condition demonstrating that cells did not just settle into the hydrogels (Figure 4a,b). These data are in line with the above described diffusions experiments (Figure S6, Supporting Information) where particles ($r = 0.5$ µm) even much smaller than T cells did not passively enter the gel. In stiffer hydrogels, such as those synthesized from 70 mg mL^{-1} Cph1*, living T cells did not migrate under either illumination condition (Figures 1b and 4b and Figure S9a, Supporting Information). The acquisition of both kinds of fluorescently labeled cells in 3D by confocal microscopy indicates that imaging can be performed through the phytochrome-based gels in the green and yellow spectrum.

c) Spatially controlled cell migration. Migration experiment was performed as in (a) except that gels were homogenously illuminated with 660 nm light (2.5 µmol m^{-2} s^{-1}) and locally with 740 nm light (100 µmol m^{-2} s^{-1}) for 15 min prior incubation in the dark for 24 h. Migration was visualized by confocal microscopy. The gel areas subjected to 660 or 740 nm illumination are indicated. Scale bar: 100 µm. d) Cell migration in response to a reversibly changing mechanical environment. Experiments were performed as in (b) except that the indicated illumination schemes were applied and only living cells were used. T cells migrated into the lower compartment were quantified by flow cytometry. $n = 6$ biological replicates. Mean is indicated. $^*P < 0.05$.

© 2019 WILEY-VCH Verlag GmbH & Co. KGaA, Weinheim

In the red spectrum this is limited due to autofluorescence of Cph1*.[12] Control experiments in nonlight-responsive Matrigel did not reveal differences in migration under either illumination condition suggesting the different light colors did not directly affect T cell migration (Figure S9b, Supporting Information).

The differential T cell migration in the phytochrome-based gel can likely not be attributed to light-dependent changes in pore size as gel pores under static, zero shear conditions were shown under either illumination condition to be significantly smaller (<102 nm, see above and Note S2, Supporting Information) than required to support T cell migration (4 μm^2 cross section, equals a diameter of ≈2.3 μm).[16] We therefore suggest that T cells are able to dynamically affect the soft hydrogel network and noncovalent protein–protein network junctions. These processes are likely dependent on the viscoelastic properties and/or stiffness of the matrix. This is in line with a recent review article about T cell mechanobiology hypothesizing that materials with stress relaxing properties (as naturally occurring tissues) might allow cells to rearrange the matrix in order to migrate despite too small pore sizes.[22b] Similarly, it has been recently demonstrated that tumor cells are able to extend invadopodia protrusions to mechanically and plastically open up micrometer-sized pores and migrate through them if the matrices are of sufficient mechanical plasticity.[25] To determine how spatially inhomogeneous mechanical properties influence the migratory response of T cells, we optically defined a path of soft hydrogel within a stiff environment by locally projecting 740 nm light onto a gel homogenously illuminated with 660 nm light of low intensity (Figure 4c). Indeed, primary activated T lymphocytes preferentially migrated through the softer path toward CXCL12/FCS (Figure 4c). Again, fixed cells used as control did not penetrate the gel at either location. These data support recent findings that T cells might seek out for the path of least resistance (tenertaxis).[24] We next investigated how T cells respond upon encountering an environment with changed mechanical properties. To this aim T cell migration was analyzed for 96 h under alternating illumination conditions with 660 and 740 nm light switched every 10 or 160 min. Rapid switching (every 10 min) prevented migration whereas longer cycles (switching every 160 min) or constant 740 nm light resulted in significantly increased cell movement, although the overall exposure time to migration-compatible 740 nm illumination was the same, namely 48 h (Figure 4d). This result suggests that in our hydrogels T cells needed a period of time before they effectively migrated upon encountering a migration-permissive environment. These findings and research approaches provide the basis to elucidate at a mechanistic level how the mechanical properties of tissues affect T cell migration and to identify extra- and intracellular processes required for T cells patrolling through the diverse mechanical environments of an organism.

In this work, we have applied concepts from optogenetics to optically tune the mechanical properties of polymer materials. The inherent biocompatibility of genetically encoded photoreceptors, combined with the advantages of using light to control processes in a fast, reversible, specific, dose- and space-dependent manner make the materials described herein a powerful tool to shed light on how cells respond to fluctuating mechanical environments. These materials pave the way for in depth, quantitative dissection of the underlying mechanosignaling mechanisms triggered by dynamic environments. The described synthesis protocol for the phytochrome-based hydrogels does likely not allow encapsulation of living cells during gel synthesis due to the long gelation time. However, we imagine that prefunctionalized polymers with phytochromes may be used for the encapsulation of living cells within minutes by light-induced formation of crosslinks. Beyond applications in research, the optical hydrogel technology described here has potential applications at the interface of life sciences and materials sciences, for example in precisely instructing stem cells in tissue engineering or in configuring the hydrogel to release drugs or other bioactive substances in a noninvasive, optically controlled manner.

Experimental Section

See the Supporting Information.

Supporting Information

Supporting Information is available from the Wiley Online Library or from the author.

Acknowledgements

The authors thank J. Schmidt, D. Schächtele, and J. Meßmer (technical facility of the Faculty of Biology, University of Freiburg) for the design and construction of the tailor-made illumination devices, R. Emig and G. Mizzon (BIOSS Toolbox) for advice in analyzing cell size and cell migration, M. Boll (University of Freiburg) for support and advice in producing Cph1*, and K. Hasis (University of Freiburg) for help with rheological measurements. The authors thank C. Groß and H. J. Wagner for critical comments and suggestions on the paper. The authors are grateful to L.O. Essen (University of Marburg, Germany) for plasmids p83 and p171 and to J. Hughes (University of Giessen, Germany) for helpful advice. Imaging was supported by the Life Imaging Center (LIC) in the Center for Systems Biology (Zentrum für Biosystemanalyse (ZBSA)), University of Freiburg. R.S. and B.H. acknowledge the financial support by the Max Planck Society, the German Research Foundation (DFG) grant SA3190, and DFG collaborative research center "Medical Epigenetics" (SFB-992). Research of W.W. was supported by the European Research Council (ERC) under the European Community's Seventh Framework Programme (FP7/2007-2013)/ERC Grant Agreement No. 259043-CompBioMat. S.M. acknowledges funding by DFG through SFB-850 (C10). W.R. acknowledges support from the Ministry of Science, Research and the Arts of Baden-Württemberg (Az: 33-7532.20), the German Federal Ministry of Education and Research in the framework of the EU ERASynBio project SynGlycTis (BMBF 031A464) and by a starting grant of the European Research Council (Programme "Ideas"—call identifier: ERC-2011-StG 282105). This work was supported by the Excellence Initiative of the German Federal and State Governments (EXC-294 (BIOSS) and GSC-4 (SGBM)). The human mesenchymal stem cells used in these experiments were purchased from Lonza.

Conflict of Interest

The authors declare no conflict of interest.

© 2019 WILEY-VCH Verlag GmbH & Co. KGaA, Weinheim

Keywords

biomaterials, cell migration, extracellular matrix, mechanosignaling, optogenetics, phytochromes

Received: October 17, 2018
Revised: January 4, 2019
Published online: January 27, 2019

[1] a) F. M. Watt, W. T. Huck, *Nat. Rev. Mol. Cell Biol.* **2013**, *14*, 467; b) P. Friedl, E. Sahai, S. Weiss, K. M. Yamada, *Nat. Rev. Mol. Cell Biol.* **2012**, *13*, 743.

[2] a) M. W. Tibbitt, C. B. Rodell, J. A. Burdick, K. S. Anseth, *Proc. Natl. Acad. Sci. USA* **2015**, *112*, 14444; b) N. Gjorevski, N. Sachs, A. Manfrin, S. Giger, M. E. Bragina, P. Ordonez-Moran, H. Clevers, M. P. Lutolf, *Nature* **2016**, *539*, 560.

[3] a) A. M. Rosales, K. S. Anseth, *Nat. Rev. Mater.* **2016**, *1*, 15012; b) J. A. Burdick, W. L. Murphy, *Nat. Commun.* **2012**, *3*, 1269; c) K. Uto, J. H. Tsui, C. A. DeForest, D. H. Kim, *Prog. Polym. Sci.* **2017**, *65*, 53; d) A. M. Kloxin, A. M. Kasko, C. N. Salinas, K. S. Anseth, *Science* **2009**, *324*, 59; e) M. Guvendiren, J. A. Burdick, *Nat. Commun.* **2012**, *3*, 792; f) C. Yang, M. W. Tibbitt, L. Basta, K. S. Anseth, *Nat. Mater.* **2014**, *13*, 645; g) R. Wang, Z. Yang, J. Luo, I. M. Hsing, F. Sun, *Proc. Natl. Acad. Sci. USA* **2017**, *114*, 5912; h) A. A. Abdeen, J. Lee, N. A. Bharadwaj, R. H. Ewoldt, K. A. Kilian, *Adv. Healthcare Mater.* **2016**, *5*, 2536.

[4] a) P. J. LeValley, A. M. Kloxin, *ACS Macro Lett.* **2019**, *8*, 7; b) N. Kong, Q. Peng, H. B. Li, *Adv. Funct. Mater.* **2014**, *24*, 7310.

[5] A. M. Rosales, S. L. Vega, F. W. DelRio, J. A. Burdick, K. S. Anseth, *Angew. Chem., Int. Ed.* **2017**, *56*, 12132.

[6] a) A. M. Rosales, K. M. Mabry, E. M. Nehls, K. S. Anseth, *Biomacromolecules* **2015**, *16*, 798; b) I. N. Lee, O. Dobre, D. Richards, C. Ballestrem, J. M. Curran, J. A. Hunt, S. M. Richardson, J. Swift, L. S. Wong, *ACS Appl. Mater. Interfaces* **2018**, *10*, 7765.

[7] A. M. Rosales, C. B. Rodell, M. H. Chen, M. G. Morrow, K. S. Anseth, J. A. Burdick, *Bioconjugate Chem.* **2018**, *29*, 905.

[8] X. L. Zhang, C. M. Dong, W. Y. Huang, H. M. Wang, L. Wang, D. Ding, H. Zhou, J. F. Long, T. L. Wang, Z. M. Yang, *Nanoscale* **2015**, *7*, 16666.

[9] L. M. Liu, J. A. Shadish, C. K. Arakawa, K. Shi, J. Davis, C. A. DeForest, *Adv. Biosyst.* **2018**, *2*, 1800240.

[10] a) S. Lyu, J. Fang, T. Duan, L. Fu, J. Liu, H. Li, *Chem. Commun.* **2017**, *53*, 13375; b) X. Wu, W. M. Huang, W. H. Wu, B. Xue, D. F. Xiang, Y. Li, M. Qin, F. Sun, W. Wang, W. B. Zhang, Y. Cao, *Nano Res.* **2018**, *11*, 5556.

[11] a) D. Tischer, O. D. Weiner, *Nat. Rev. Mol. Cell Biol.* **2014**, *15*, 551; b) K. Kolar, C. Knobloch, H. Stork, M. Znidaric, W. Weber, *ACS Synth. Biol.* **2018**, *7*, 1825.

[12] J. Mailliet, G. Psakis, K. Feilke, V. Sineshchekov, L. O. Essen, J. Hughes, *J. Mol. Biol.* **2011**, *413*, 115.

[13] M. Adrian, W. Nijenhuis, R. I. Hoogstraaten, J. Willems, L. C. Kapitein, *ACS Synth. Biol.* **2017**, *6*, 1248.

[14] M. Lekka, D. Gil, K. Pogoda, J. Dulinska-Litewka, R. Jach, J. Gostek, O. Klymenko, S. Prauzner-Bechcicki, Z. Stachura, J. Wiltowska-Zuber, K. Okon, P. Laidler, *Arch. Biochem. Biophys.* **2012**, *518*, 151.

[15] H. M. Beyer, O. S. Thomas, N. Riegel, M. D. Zurbriggen, W. Weber, M. Hörner, *Acta Biomater.* **2018**, *79*, 276.

[16] K. Wolf, M. Te Lindert, M. Krause, S. Alexander, J. Te Riet, A. L. Willis, R. M. Hoffman, C. G. Figdor, S. J. Weiss, P. Friedl, *J. Cell Biol.* **2013**, *201*, 1069.

[17] T. T. Lee, J. R. Garcia, J. I. Paez, A. Singh, E. A. Phelps, S. Weis, Z. Shafiq, A. Shekaran, A. Del Campo, A. J. Garcia, *Nat. Mater.* **2015**, *14*, 352.

[18] a) T. Yeung, P. C. Georges, L. A. Flanagan, B. Marg, M. Ortiz, M. Funaki, N. Zahir, W. Ming, V. Weaver, P. A. Janmey, *Cell Motil. Cytoskeleton* **2005**, *60*, 24; b) A. Engler, L. Bacakova, C. Newman, A. Hategan, M. Griffin, D. Discher, *Biophys. J.* **2004**, *86*, 617; c) O. Chaudhuri, L. Gu, M. Darnell, D. Klumpers, S. A. Bencherif, J. C. Weaver, N. Huebsch, D. J. Mooney, *Nat. Commun.* **2015**, *6*, 6364; d) O. Chaudhuri, L. Gu, D. Klumpers, M. Darnell, S. A. Bencherif, J. C. Weaver, N. Huebsch, H. P. Lee, E. Lippens, G. N. Duda, D. J. Mooney, *Nat. Mater.* **2016**, *15*, 326; e) B. Venugopal, P. Mogha, J. Dhawan, A. Majumder, *Biomater. Sci.* **2018**, *6*, 1109.

[19] a) J. Hao, Y. L. Zhang, D. Jing, Y. Shen, G. Tang, S. S. Huang, Z. H. Zhao, *Acta Biomater.* **2015**, *20*, 1; b) Q. Chen, P. Shou, C. Zheng, M. Jiang, G. Cao, Q. Yang, J. Cao, N. Xie, T. Velletri, X. Zhang, C. Xu, L. Zhang, H. Yang, J. Hou, Y. Wang, Y. Shi, *Cell Death Differ.* **2016**, *23*, 1128; c) C. X. Li, N. P. Talele, S. Boo, A. Koehler, E. Knee-Walden, J. L. Balestrini, P. Speight, A. Kapus, B. Hinz, *Nat. Mater.* **2017**, *16*, 379.

[20] a) S. Dupont, L. Morsut, M. Aragona, E. Enzo, S. Giulitti, M. Cordenonsi, F. Zanconato, J. Le Digabel, M. Forcato, S. Bicciato, N. Elvassore, S. Piccolo, *Nature* **2011**, *474*, 179; b) A. Elosegui-Artola, I. Andreu, A. E. M. Beedle, A. Lezamiz, M. Uroz, A. J. Kosmalska, R. Oria, J. Z. Kechagia, P. Rico-Lastres, A. L. Le Roux, C. M. Shanahan, X. Trepat, D. Navajas, S. Garcia-Manyes, P. Roca-Cusachs, *Cell* **2017**, *171*, 1397.

[21] a) J. L. Balestrini, S. Chaudhry, V. Sarrazy, A. Koehler, B. Hinz, *Integr. Biol.* **2012**, *4*, 410; b) P. C. Dingal, A. M. Bradshaw, S. Cho, M. Raab, A. Buxboim, J. Swift, D. E. Discher, *Nat. Mater.* **2015**, *14*, 951.

[22] a) I. Levental, P. C. Georges, P. A. Janmey, *Soft Matter* **2007**, *3*, 299; b) A. de la Zerda, M. J. Kratochvil, N. A. Suhar, S. C. Heilshorn, *APL Bioeng.* **2018**, *2*, 021501.

[23] M. Saitakis, S. Dogniaux, C. Goudot, N. Bufi, S. Asnacios, M. Maurin, C. Randriamampita, A. Asnacios, C. Hivroz, *eLife* **2017**, *6*, e23190.

[24] R. Martinelli, A. S. Zeiger, M. Whitfield, T. E. Sciuto, A. Dvorak, K. J. Van Vliet, J. Greenwood, C. V. Carman, *J. Cell Sci.* **2014**, *127*, 3720.

[25] K. M. Wisdom, K. Adebowale, J. Chang, J. Y. Lee, S. Nam, R. Desai, N. S. Rossen, M. Rafat, R. B. West, L. Hodgson, O. Chaudhuri, *Nat. Commun.* **2018**, *9*, 4144.

© 2019 WILEY-VCH Verlag GmbH & Co. KGaA, Weinheim